Ultralow-loss optical diamagnetism in silver nanoforests

J. Opt. A: Pure Appl. Opt. **11** (2009) 114026 (9pp) doi:10.1088/1464-4258/11/11/114026

Ultralow-loss optical diamagnetism in silver nanoforests

J J H Cook, K L Tsakmakidis and O Hess

Advanced Technology Institute and Department of Physics, Faculty of Engineering and Physical Sciences, University of Surrey, Guildford GU2 7XH, UK

E-mail: O.Hess@surrey.ac.uk

Received 7 April 2009, accepted for publication 4 June 2009
Published 17 September 2009
Online at stacks.iop.org/JOptA/11/114026

Abstract

A comprehensive investigation of the optical properties of a composite metamaterial in which silver nanowires are aligned inside a *finite-thickness* dielectric host medium is presented. Using a rigorous finite-element based modelling approach, together with a self-consistent process for the extraction of effective-medium parameters, we find that this structure can enable an effective *optical* diamagnetic response that is orders of magnitude stronger compared to that of naturally occurring diamagnetic materials. Interestingly, our analysis reveals that there is a frequency region where the nanoforest exhibits a strong diamagnetic response while *simultaneously* allowing for *high transmission* of incident electromagnetic waves. We examine the physical origin behind the magnetic properties of this structure, as well as its resilience to fabrication imperfections. Our analysis shows that the structure is robust to the presence of disorder, in the occurrence of which it can still facilitate high figure-of-merit diamagnetic responses.

Keywords: diamagnetism, metamaterials, plasmonics, disorder, finite element modelling

(Some figures in this article are in colour only in the electronic version)

1. Introduction

Metamaterials are engineered media that owe their electromagnetic properties to their chemical composition *and* the structure of their (subwavelength) 'metamolecules'. As the periodic table only has a finite number of chemical elements, engineering the electromagnetic response of a medium by suitable structuring of its 'metamolecules' allows for overcoming a variety of limitations pertaining to naturally occurring materials, and entering regimes where, e.g., the (effective) refractive index of a medium can now become negative—a property never found in nature.

The first metamaterial was a combination of magnetic metamolecules, made of so-called split-ring resonators [1], and electric metamolecules made of thin metal wires [2]. That structure was shown to exhibit an effective negative refractive index (NRI) in the microwave regime [2]. The experimental demonstration of a NRI medium in the microwave regime led to a profound resurgence of interest in the properties of these composite media, as well as to continuous efforts towards scaling them to higher frequencies in order to realize and harness their unique optical properties [3–6] across a broad spectrum.

Obtaining a metamaterial response (e.g., diamagnetism or NRI) at higher frequencies is challenging, not least because of the modification of the electromagnetic properties of metals at optical frequencies, the absence of high-permittivity dielectric hosts [7] and the fabrication difficulties associated with the correspondingly small periodicities and features of the metamolecules [8]. Moreover, considerations such as bandwidth, dissipative losses and disorder also need to be included in the analysis before a useful metamaterial design can be reached.

The aforementioned realizations have led to the investigation and proposal of a variety of metamaterial designs. Structures investigated thus far towards obtaining optical magnetism and/or negative refractive index include the so-called fishnet design (metal/dielectric layers) [9], short (cut) metallic wires [10], plasmonic nanorings [11] and chiral metallic crosses [12].

Significantly less research has focused on the potential of metamaterials for enabling *low-loss* diamagnetism, with previous studies [13, 14] focusing on well ordered and infinitely periodic arrays of plasmonic nanoparticles, in which the obtained figures of merit ($\mathrm{Re}\{\mu\}/\mathrm{Im}\{\mu\}$, μ being the effective magnetic permeability of the metamaterial) were

typically of the order of unity. Considering that most naturally occurring diamagnetic media are characterized by magnetic susceptibilities χ of the order of only $\sim -10^{-5}$ (with the exception of superconductors, which are perfect diamagnets with $\chi = -1$), *low-loss* diamagnetic metamaterials may find important potential applications, e.g., in enabling room-temperature (dia)magnetic levitation.

In the following we are studying a metamaterial nanocomposite that can facilitate *ultralow-loss* diamagnetic responses, even in the presence of disorder, by virtue of its suitably engineered structure. The metamaterial is an anisotropic formation of silver nanowires ('silver nanoforest') embedded in a dielectric host medium, and can be straightforwardly realized using existing, mature metamaterial technology [15, 16]. In this structure the area of the metal–dielectric interfaces is large (compared with the volume of a metal wire); hence, it is expected that the effective electromagnetic response of this medium should be greatly affected by the presence of surface plasmon polaritons (SPPs) [17, 18]—quasi-particles formed by light being coupled to oscillating electrons on the surface of a negative-permittivity material, such as a plasmonic wire. The coupling of light to supported SPP modes confines it to the interface of the metallic–dielectric inclusions and allows unusual subwavelength features to emerge, including extraordinary transmission of light through subwavelength holes in metal surfaces [19]. As we shall discover in the following, placing aligned silver nanowires inside a finite-thickness dielectric host allows for the existence and mutual coupling of SPP modes, the latter having a profound effect on the overall (averaged/effective) magnetic response of the structure, leading ultimately to frequency regions with high transmission and *negative* magnetic susceptibilities ($\chi < 0$ and $0 < \mathrm{Re}\{\mu\} < 1$).

2. Computational methodology

To rigorously analyse the optical properties of the nanostructured plasmonic arrangements, we deploy a vectorial, adaptive finite-element simulation methodology [20], combined with proper perfectly matched layer (PML) absorbing, radiation and periodic boundary conditions, which allow us expediently and with high accuracy to obtain the scattering spectra of our structure. The nanowires shown in figure 1 are assumed to extend infinitely in the horizontal (x) and vertical (z) directions, with a horizontal centre-to-centre spacing fixed to $\Delta x = 36$ nm (in *all* cases), radius $r = 5$ or 10 nm, and longitudinal spacing of $\Delta y = 12$, 22 or 24 nm. Crucial for the manifestation of low-loss diamagnetism in this structure is, as we shall discover in the following, the fact that its thickness (t_{cell}) along the y-direction is *finite*.

Our structure is illuminated by a transverse electromagnetic (TEM) plane wave (E_x, H_z), propagating along the $+y$ direction (normal incidence). *Longitudinal* (i.e. *parallel* to the wires' axes) transverse magnetic (TM) incidence into an array of silver nanowires that was embedded inside an alumina matrix has previously been studied theoretically [21] and experimentally [15] and was shown to enable negative refraction—

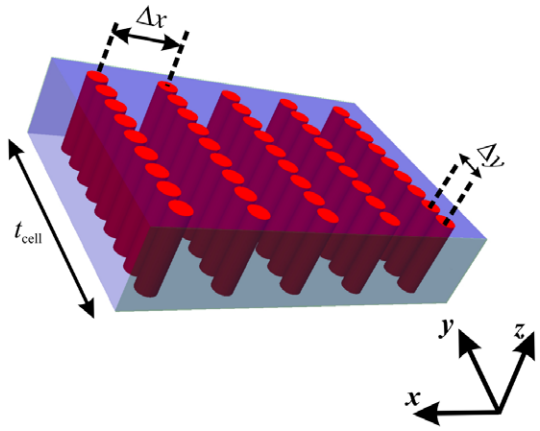

Figure 1. Schematic illustration of the three-dimensional geometrical structure of the diamagnetic metamaterial. Also shown is the thickness of a unit cell (t_{cell}) along the direction of light propagation.

but *not* negative effective refractive index or negative effective permittivity or permeability.

The real (ε') and imaginary (ε'') parts of the permittivity of the silver nanowires were, respectively, modelled using the following Drude–Sommerfeld relations:

$$\varepsilon' = 1 - \frac{\omega_{\mathrm{p}}^2 \tau^2}{1 + \omega^2 \tau^2}, \tag{1}$$

$$\varepsilon'' = \frac{\omega_{\mathrm{p}}^2 \tau^2}{\omega(1 + \omega^2 \tau^2)}, \tag{2}$$

with $\omega_{\mathrm{p}} = 9.8 \times 10^{15}$ s^{-1} being the plasma frequency of the metal, $\tau = 3.1 \times 10^{-14}$ s the relaxation time of the electrons in the metal and ω the angular frequency of the incoming EM wave. The values for ω_{p} and τ were derived from the experimental data of Johnson and Christy [22]. The dielectric background was assumed to be lossless and have a constant, frequency independent, permittivity of $\varepsilon_{\mathrm{b}} = 6.52$ (glass).

3. Retrieval of the metamaterial effective constitutive parameters

The adaptive-mesh finite-element simulation methodology [20] allows one to expediently obtain the (steady state) electric and magnetic field spatial distributions, as well as the reflection and transmission of a perpendicularly (to our structure) incident electromagnetic wave for a variety of optogeometric set-ups and wavelengths. From these results it is possible to compute the effective parameters (permittivity, permeability and refractive index) [23] of our diamagnetic metamaterial using the methodology that is outlined in the following.

Assuming that the finite-thickness metamaterial can (in the long-wavelength, quasi-static regime) be described as a homogeneous slab of thickness d (t_{cell} in figure 1), one can use the numerically calculated (complex) reflection (r) and transmission (t) coefficients associated with this structure in order to derive its effective refractive index (n) based on the

following relations [23]:

$$\mathrm{Im}(n) = \pm\,\mathrm{Im}\left(\frac{\arccos\{\frac{1}{2t'}[1-(r^2-t'^2)]\}}{kd}\right), \quad (3)$$

$$\mathrm{Re}(n) = \pm\,\mathrm{Re}\left(\frac{\arccos\{\frac{1}{2t'}[1-(r^2-t'^2)]\}}{kd}\right) + \frac{2\pi m}{kd}, \quad (4)$$

with k being the wavenumber of the incident electromagnetic wave and $t' = te^{ikd}$ the normalized transmission coefficient. Note that in equation (4) there is an ambiguity in the value that should be chosen for the integer number m—but there is *no* such ambiguity in equation (3), which gives the imaginary part of the structure's effective refractive index. Prompted by this observation, in our calculations of the various structures' effective parameters we use the *unambiguously* calculated $\mathrm{Im}(n)$ (equation (3)) in order to make an initial estimation of $\mathrm{Re}(n)$ via the following Kramers–Kronig relation:

$$\mathrm{Re}(n(\omega)) = 1 + \frac{2}{\omega}P\int_0^\infty \frac{\omega'\,\mathrm{Im}(n(\omega'))}{\omega'^2-\omega^2}\partial\omega', \quad (5)$$

where P denotes the Cauchy principal value. In equation (5) one should use a sufficiently wide range of frequencies to ensure that the integral converges at every angular frequency ω. Then, equation (5) can be reliably deployed as a guide in determining the correct branch (value of integer m) of $\mathrm{Re}(n)$. This self-contained and consistent methodology guarantees the causal character of the extracted effective refractive indices, while obviating the need for examining structures with various thicknesses before a reliable estimation of n can be reached. Indeed, in *all* of the results presented below we have found *excellent* agreement between the values of $\mathrm{Re}(n)$ obtained from equation (4) (with a correctly identified value of m) and equation (5).

From the numerically calculated reflection and transmission coefficients one can, also, determine the effective impedance (Z) of the structure using the following relation [23]:

$$Z = \pm\sqrt{\frac{(1+r)^2-t'^2}{(1-r)^2-t'^2}}. \quad (6)$$

Since there are no gain media present in the metamaterial structure, the real part of its (complex) impedance is always *set* to be positive. A similar requirement holds for the imaginary part of the structure's effective refractive index, which should also be positive since the structure is overall passive. Finally, having calculated the metamaterial's effective refractive index (n) and impedance (Z), one can use equation (7) below to extract its effective magnetic permeability (μ):

$$\mu = nZ. \quad (7)$$

Equation (7) is the formula used in the derivation of all the results presented below pertaining to the ultralow-loss diamagnetic behaviour of the metamaterial structure described in section 2.

4. Optical magnetism in silver nanoforest metamaterials

Silver is itself a weakly diamagnetic material having a (negative) magnetic susceptibility that is approximately equal to $\chi_m \approx -2.64\times10^{-5}$, depending greatly upon its purity—in particular, its freedom from traces of ferromagnetic impurities. In the following we are showing that an arrangement of tightly coupled silver nanowires, embedded inside a glass host, results (in a certain frequency region) in an effective diamagnetic metamaterial having four orders of magnitude stronger diamagnetic response ($0.3 < \mathrm{Re}\{\mu\} = \mu_r < 0.9$), while *simultaneously* exhibiting *ultralow* magnetic losses ($\mathrm{Re}\{\mu\}/\,\mathrm{Im}\{\mu\} = \mu_r/\mu_i \approx 60$–$460$).

Figure 2(a) reports the numerically calculated transmission coefficient (t) of a nanostructure (figure 1) in which the silver wires are only 2 nm apart in the longitudinal (y) direction and 26 nm apart in the horizontal (x) direction. One immediately observes from this figure that there are successive regions (shown in red colour) of high (*above* 80–90%) and broadband Fabry–Perot-/antireflection-coating-like transmission, owing to the finite thickness of the dielectric host medium. The presence of a dense array of silver nanowires does not destroy the overall transmission characterizing the dielectric host in these regions and, as we shall see later (figure 2(b)), has a profound impact on the effective magnetic response of the metamaterial nanostructure. We further note from figure 2(a) that there are three distinct (bandgap) regions (shown in dark blue colour) of very low transmission, occurring for wavelengths below approximately 450 nm, between 490 and 580 nm, and at approximately 675 nm. The spectral width of these regions remains unaffected by variations in the thickness of the nanostructure; i.e., adding more nanowires in the longitudinal (y) direction does not influence the spectral range over which these photonic bandgap regions occur, since the bandgaps (which are fully established for a sufficiently thick structure) are indeed expected to arise over only certain wavelength regions.

Figure 2(b) reports the extracted (following the methodology of section 3) real part of the effective relative permeability of a 128 nm thick silver nanoforest. Also shown in the same graph is the transmission coefficient characterizing the structure over the examined wavelength region (400–1200 nm). For small wavelengths (400—500 nm) one finds that the structure supports coupled SPP resonances, similar in nature to bulk surface plasmon modes existing around 450 nm. As we shall discover in the following, these modes are almost insensitive to the particular geometrical features and positioning of the nanowires (separation distances, radii, etc) and are responsible for facilitating increased transmission of an incident light wave through the structure. For the particular structure shown in figure 2(a), the occurrence of such modes disrupts the spectral continuity of the SPP photonic bandgap region, which (if these coupled SPP modes were, by some means, suppressed) would extend continuously from 400 to 550 nm. We note that the presence of the coupled SPP resonances results, here, in an overall transmission (through both interfaces of the finite-thickness nanostructure) of up to approximately 40%. It should

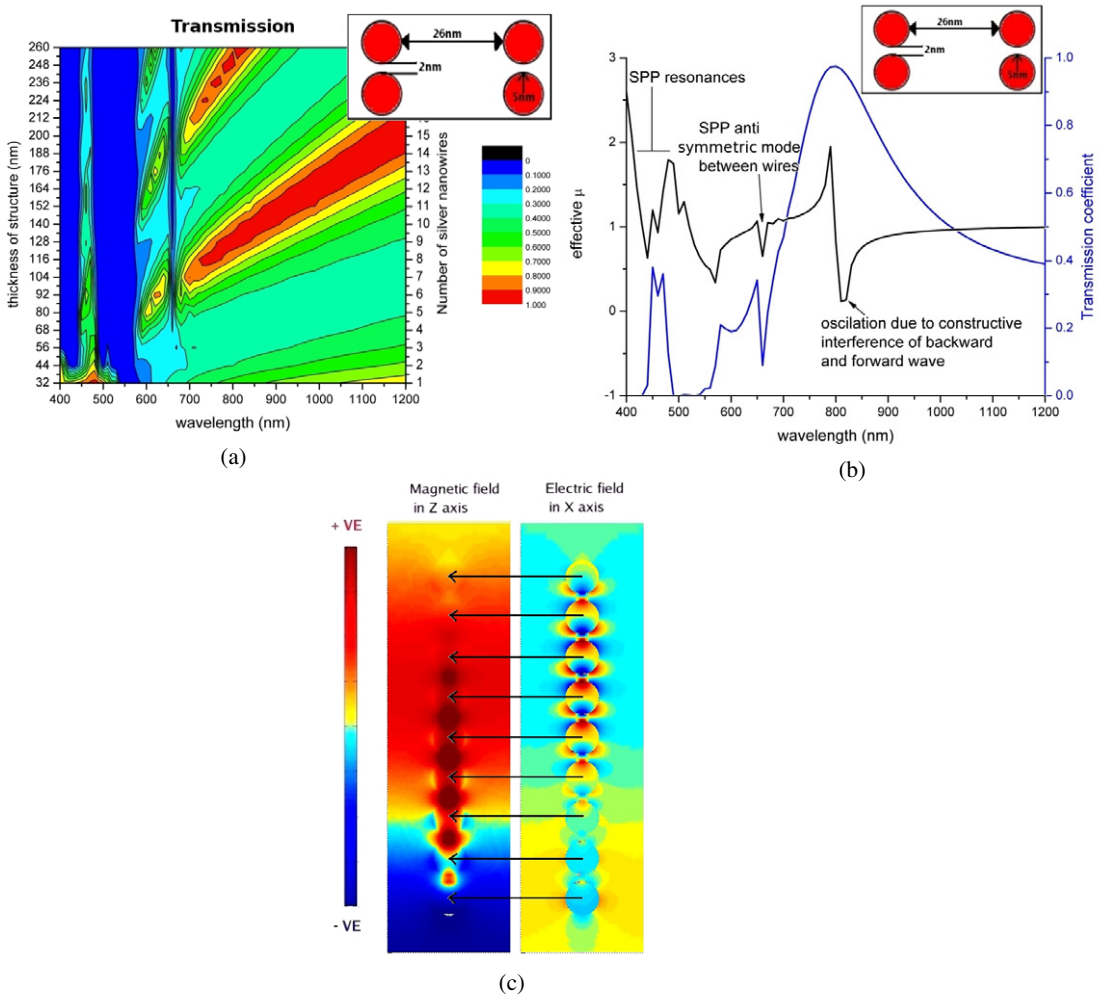

Figure 2. In all cases it is assumed that the silver nanowires are embedded inside a finite-thickness glass host, they have radius of 5 nm, and they are separated by 26 nm in the horizontal x-direction and by 2 nm in the longitudinal y-direction, as shown in the top insets of (a) and (b). (a) Contour plot of the transmission coefficient versus wavelength for silver nanoforests of various thicknesses. (b) Real part of effective relative permeability (black line) and transmission coefficient (blue line) for a 128 nm thick silver nanostructure. (c) Snapshot of the propagation of the magnetic (left) and electric (right) field component inside a 128 nm thick nanoforest for an incident light wavelength of 660 nm.

also be noted that the extracted effective magnetic permeability μ of the structure in wavelength regions where a bandgap occurs cannot reliably characterize the effective (averaged) magnetic behaviour of the structure in these regions, owing to the sensitivity of the extracted parameters to possible small numerical errors when the transmission $t \approx 0$ (see equations (3) and (4)). These bandgap regions, however, are not of interest here (not least because the structure does not facilitate any appreciable transmission within these regions), since here we are focusing on long-wavelength and non-zero-transmission regions where an effective magnetic description of our structure(s) can, indeed, be meaningful.

From figure 2(b) we, further, observe that above the SPP bandgap region the transmission of incident lightwaves through the nanostructure progressively (though not monotonically) increases with wavelength, up to a spectral region centred at 660 nm. At $\lambda = 660$ nm a sharp dip appears in the transmission spectrum of the nanoforest, accompanied by a corresponding dip in the variation with wavelength of its effective permeability. The origin of this feature is elucidated with the aid of figure 2(c), which illustrates a snapshot of the propagation of the magnetic and electric field components through the nanostructure. One clearly observes the presence of highly localized electric fields at the surfaces of the nanowires—similar in nature to the localized SPP resonances that were occurring at smaller wavelengths, and were responsible for the reduction of the transmission through the nanostructure. Furthermore, the localized electric fields flip sign between adjacent nanowires. As a result, they form closed displacement–current loops on the xy-plane (see figure 1), thereby inducing (z-directed) magnetic dipole moments *between* the nanowires [24]. These magnetic moments are (on average) directed *oppositely* to the incident magnetic field; hence, they are responsible for the weak diamagnetic dip that is observed at $\lambda = 660$ nm in the plot of the structure's effective permeability versus wavelength (figure 2(b)). It is, also, to be noted from figure 2(c) that the wavelength of the lightwave *inside* the nanostructure is much

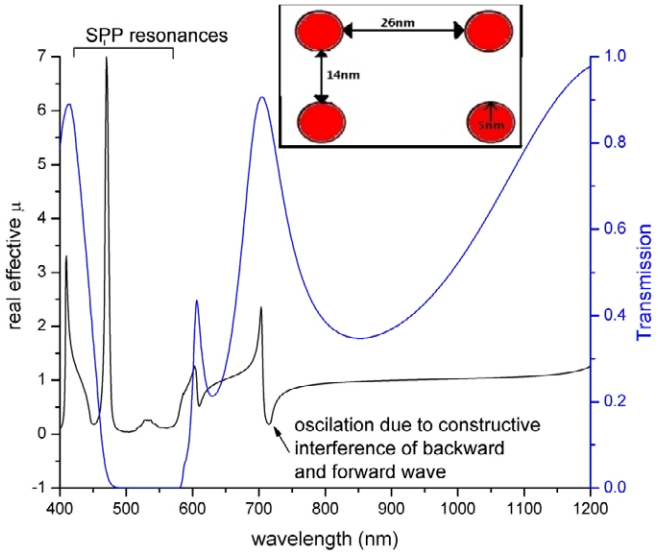

Figure 3. Here, it is assumed that the silver nanowires are embedded inside a finite-thickness glass host, they have radius of 5 nm, and they are separated by 26 nm in the horizontal x-direction and by 12 nm in the longitudinal y-direction, as shown in the top inset. Shown is the real part of the effective relative permeability (black line) and transmission coefficient (blue line) for a 218 nm thick silver nanostructure.

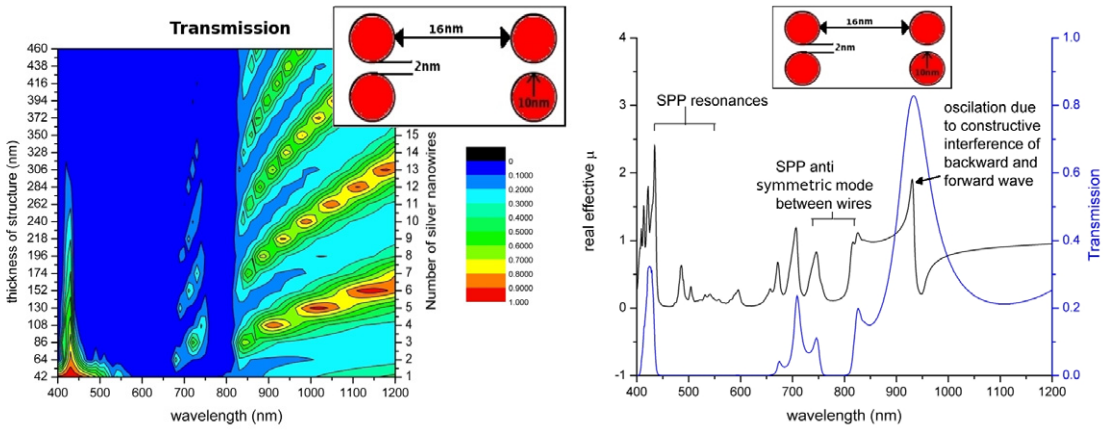

Figure 4. In all cases it is assumed that the silver nanowires are embedded inside a finite-thickness glass host, they have radius of 10 nm, and they are separated by 16 nm in the horizontal x-direction and by 2 nm in the longitudinal y-direction, as shown in the top insets of (a) and (b). (a) Contour plot of the transmission coefficient versus wavelength for silver nanoforests of various thicknesses. (b) Real part of effective relative permeability (black line) and transmission coefficient (blue line) for a 218 nm thick silver nanostructure.

larger than the periodicity (particularly along the z-direction), i.e. we are well within the 'effective-medium'/quasi-static regime. Thus, the assignment of bulk effective electromagnetic parameters to the nanostructure in this region is, indeed, meaningful.

A particularly interesting (and reoccurring; see also figures 3–5 below) feature of the silver nanoforest is the existence of a spectral region where both a strong diamagnetic response *and* high transmission are simultaneously achieved. The origin of this feature, which in figure 2(b) exists at around 800 nm, is explained as follows: When the nanowires are not embedded inside the finite-thickness glass host, the resulting dielectric heterostructure (slab of glass surrounded by air) behaves, at 800 nm, similarly to an antireflection coating, i.e. it supports Fabry–Perot-like modes that interfere destructively in the backward direction and constructively in the forward direction. As a result, the transmission of incident lightwaves through the heterostructure in that spectral region approaches 100%. Furthermore, since the heterostructure is purely dielectric, its effective relative magnetic permeability (extracted following, e.g., the methodology of section 3) is *unity for all wavelengths*, as expected. When one immerses the nanowires inside the glass slab in such a way that their separation distance in the horizontal x-direction is $d > 4r$, r being the nanowire radius (see the inset in figure 2(b)), the transmission property of the resulting plasmonic nanostructure is still close to 100%, as shown in figure 2(b), i.e. it is only slightly affected (at 800 nm) by the presence of the nanowires

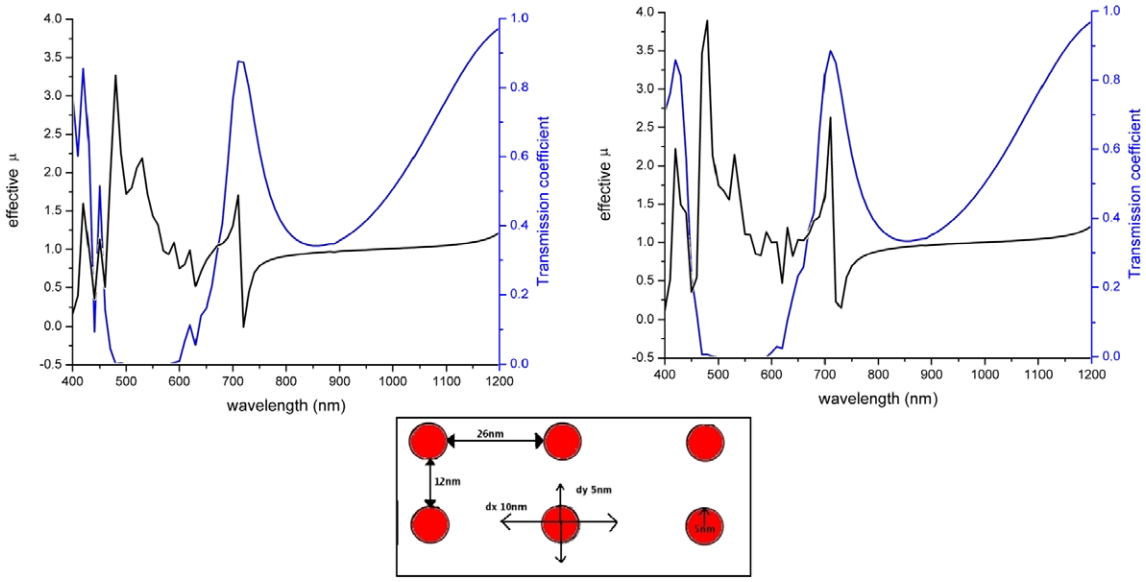

Figure 5. Here, it is assumed that the silver nanowires are embedded inside a finite-thickness glass host, they have radius of 5 nm, they are initially separated by 26 nm in the horizontal x-direction and by 12 nm in the longitudinal y-direction, and they are displaced from their perfectly periodic position by up to 10 nm in the x-direction and by up to 5 nm in the z-direction, as shown in the bottom inset. In both figures (above) shown are the real parts of the effective relative permeability (black line) and the transmission coefficient (blue line) for two 218 nm thick silver nanostructures, in which each nanowire was allowed to *randomly* move away from its initial position.

compared with the all-dielectric heterostructure. This is because the incident lightwaves are still able to propagate (and interfere) through the nanostructure via the (sufficiently wide) dielectric regions between the columns of nanowires, thereby resulting in an overall transmission that is again close to 100% (at $\lambda = 800$ nm). However, despite the fact that the transmission property of the nanostructure remains almost unchanged (at $\lambda = 800$ nm) when the nanowires are introduced inside the glass host, the magnetic response of the resulting plasmonic metamaterial is, indeed, profoundly affected by the presence of the nanowires. For instance, as we see from figure 2(b) the effective relative magnetic permeability of the nanostructure deviates strongly from unity in the spectral region centred at 800 nm. In particular, above 800 nm the structure exhibits a strong diamagnetic response, while simultaneously allowing for high transmission of incident lightwaves. This property directly results in effective (relative) permeabilities μ whose real parts are smaller than unity and much larger than the corresponding imaginary parts (figure of merit FOM $= \mathrm{Re}\{\mu\}/\mathrm{Im}\{\mu\} \gg 1$). For instance, at $\lambda = 820$ nm we obtain $\mathrm{Re}\{\mu\} = 0.777\,89$ with FOM $=$ 133.888, while at $\lambda = 830$ nm we have $\mathrm{Re}\{\mu\} = 0.883\,28$ with FOM $= 462.45$.

Figure 3 reports the effective (relative) magnetic permeability and transmission property of a nanostructure similar to that of figure 2, but with the distance between the nanowires in the longitudinal y-direction increased (from 2 nm) to 14 nm. This geometric arrangement results in a reduced nanowire unit cell filling factor, i.e. in more dielectric (glass) being present in the composite medium. For this reason some of the *localized* surface plasmon resonances that were previously (in figure 2) occurring at small wavelengths are now absent, and the structure facilitates an increased transmission of up to 90% in the spectral region 400–450 nm. The SPP bandgap region now extends from 480 to 575 nm; beyond it there are no antisymmetric SPP modes, nor any appreciable (induced) magnetic moments occurring (as in figure 2). This is a consequence of the increased area between the nanowires, that diminishes the strength of these weak (in amplitude) magnetic moments. However, we note from figure 3 that the nanostructure still supports an *ultralow-loss diamagnetic* response in a spectral region above 700 nm, which is similar in nature to that identified and explained previously in figure 2. In this region one obtains yet again effective (relative) permeabilities μ with very good figures of merit and with real parts being appreciably smaller than unity. For instance, at $\lambda = 720$ nm we find $\mathrm{Re}\{\mu\} = 0.346\,66$ with FOM $=$ 150.7217, while at $\lambda = 730$ nm it is $\mathrm{Re}\{\mu\} = 0.669\,43$ with FOM $= 249.7873$.

Finally, figure 4 reports the effect that increasing the radii of the nanowires and decreasing their separation distance in the horizontal x-direction has on the transmission property and magnetic response of the silver nanoforest. One finds from figure 4(a) that the SPP bandgap region is *fully* established for nanostructure thicknesses above approximately 350 nm. As expected, this bandgap region is now much wider compared to, e.g., the corresponding region occurring for the nanostructure of figure 2; here, it extends from 400 up to 820 nm. The only useful magnetic property of the composite medium that survives from such a tight coupling of (relatively) 'thick' plasmonic nanowires is its high figure-of-merit diamagnetic response, which here is red-shifted to around 950 nm. The red-shift in the diamagnetic response of our structure(s) when the radius of the nanowires or the nanowire density increases is because, in both cases, the increased presence of the plasmonic inclusions raises the effective refractive index of the

structure(s); hence, the wavelength *inside* our structure(s) is, in both cases, reduced and therefore the diamagnetic response is, now, expected to occur at higher *free-space* wavelengths. For the structure of figure 4, in the spectral region around 950 nm we are, once more, able to harness high transmissions (above or around 80%) *and* strong diamagnetic responses from our plasmonic metamaterial. For instance, at $\lambda = 960$ nm we obtain $\mathrm{Re}\{\mu\} = 0.483\,28$ with FOM $= 138.4756$, while at $\lambda = 970$ nm we have $\mathrm{Re}\{\mu\} = 0.625\,47$ with FOM $= 163.3081$.

5. Effect of disorder on the diamagnetic response of the silver nanoforest

Thus far, in all of the presented results, we have assumed that the nanowires are embedded inside the glass host in a perfectly periodic and orderly fashion. However, any experimentally realized nanostructure will posess some degree of structural imperfections, such as disorder (e.g. in the positioning of the nanowires), roughness on the surface of the cylindrical nanowires, and so forth. It is well known from extensive theoretical and experimental studies pertaining to the transport properties of electric (conductive) or optical materials that these media can be adversely affected by the presence of disorder. For instance, the presence of disorder can phase-change a conductor to a non-absorbing insulator, a phenomenon known as Anderson localization [25]—originating from interference of multiply (elastically) scattered electron-waves inside the disordered conductor. The same phenomenon can also occur in disordered dielectric media [26]. Further, in photonic crystal line-defect waveguides, disorder can cause a shift in the cut-off of the guided modes [27], thereby resulting in strong reflection (backscattering) losses that dominate over all other types of losses (e.g. dissipative). It is, thus, essential to herein study the effect that disorder may have on the magnetic properties of the considered silver nanoforest; in particular, the extent to which disorder can affect the afore-described ultralow-loss diamagnetic response of our nanoplasmonic metamaterial.

To this end, we consider the nanostructures shown in figure 5, where silver nanowires with a radius of 5 nm are separated by 26 nm in the horizontal x-direction, and by 12 nm in the longitudinal y-direction. In our finite-element simulations we allow *each* nanowire to *randomly* move from its initial position by up to 10 nm in the x-direction (rightwards or leftwards) and by up to 5 nm in the y-direction (upwards or downwards), as illustrated in the bottom inset of figure 5. This choice for the random displacement of the nanowires from their central location is sufficient to cause substantial positional disorder in the nanostructure, while simultaneously assuring that none of the wires will overlap with its neighbours.

The transmission properties and extracted effective permeabilities for two such (disordered) nanostructures are reported in figure 5. We note that the properties of both structures remain similar to the corresponding properties of the nanostructure that was studied in figure 3. In particular, both metamaterial structures in figure 5 are characterized by a low-wavelength spectral region where the transmission of incident lightwaves is high, followed by an SPP bandgap region, which extends approximately from 500 to 600 nm. Above this region, one may obtain very high transmission (centred at ∼700 nm) of up to 90%, accompanied by a strong diamagnetic response. The antireflection-coating-like, ultralow-loss nature of the diamagnetic behaviour of the two disordered nanostructures in figure 5 is identical with the low-loss nature of the diamagnetic responses of the structures studied previously in figures 2–4. The only feature that was present in figure 3 and does not survive from the strong disorder present in the nanosystems of figure 5 is, in fact, the occurrence of a negative effective permeability in a narrow region just before the onset of the SPP bandgap region in figure 3(a).

That feature, which was only very weakly present in the nanostructure of figure 3, is indeed adversely affected by the presence of disorder, since it is absent from the effective-μ responses of both structures in figure 5.

Figure 6 presents the transmission and effective magnetic properties of two silver nanoforests in which wires of 10 nm radius are separated by 16 nm in the horizontal direction and by (only) 2 nm in the longitudinal direction, as illustrated in the bottom inset of figure 6. In this structure, the nanowires are displaced by up to 5 nm from their perfectly periodic position *only* along the horizontal direction (leftwards or rightwards). Despite the fact that these two nanostructures are characterized by a smaller degree of disorder compared with the structures of figure 5, the tight coupling of the nanowires in the y-direction, combined with the increase in the radii of the wires, result (when the afore-described disorder is present) in an almost complete obliteration of any useful property of this system—including the low-loss diamagnetic response. The maximum transmission of incident lightwaves through the disordered systems of figure 6 is approximately 40%–45%, occurring (for both structures) at around 950 nm. However, even in this spectral region of relatively high transmission, the effective-μ behaviour of the structures is erratic and cannot be deployed for the production of low-loss magnetic metamaterials with robust and repeatable performance.

6. Conclusions

We have presented a detailed analysis of the magnetic properties of arrays of silver nanowires, embedded in dielectric (glass) slabs. Our analysis has revealed that these structures can facilitate (room-temperature) ultralow-loss diamagnetic responses in the visible (figures 3 and 5) and near-infrared (figures 2, 4–6) regimes. The ultralow-loss behaviour is achieved by constructing the structures such that they are sufficiently small in the longitudinal direction (so that dissipative light attenuation is not the primary source of losses) and almost perfectly impedance-matched to the surrounding free space. With these structures one can obtain diamagnetic responses that are orders of magnitude stronger compared to naturally occurring media, while simultaneously achieving figures of merit that can be several hundreds (again, orders of magnitude better than the figures of merit normally obtained for negative-μ metamaterials). Furthermore, the low-loss diamagnetic responses of the studied nanostructures turn out to be resilient to the presence of even strong positional

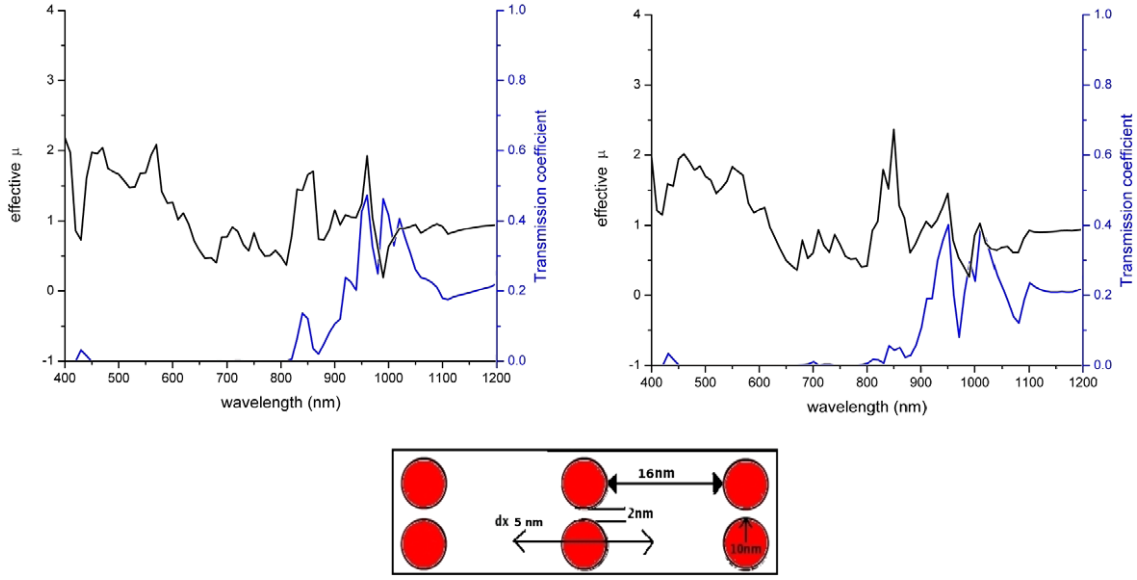

Figure 6. Here, it is assumed that the silver nanowires are embedded inside a finite-thickness glass host, they have radius of 10 nm, they are initially separated by 16 nm in the horizontal x-direction and by (only) 2 nm in the longitudinal y-direction, and they are displaced from their perfectly periodic position by up to 5 nm in the x-direction only, as shown in the bottom inset. In both figures (above) shown are the real parts of the effective relative permeability (black line) and the transmission coefficient (blue line) for two 218 nm thick silver nanostructures, in which each nanowire was allowed to *randomly* move away from its initial position.

disorder, so long as the nanowires are not very tightly coupled in the direction in which the incident lightwave propagates inside the structure. As such, these nanosystems can (when illuminated by light of appropriate frequency) potentially find a wealth of useful applications in magnetic circuits, magnetic isolation (for equipments designed to make sensitive magnetic measurements) [28], diamagnetic levitation of small (nanometre-scale) substances, magnetic-field-induced alignment of liquid crystals and mesoporous inorganic materials (such as silica) [29], and so forth.

References

[1] Pendry J B, Holden A J, Robbins D J and Stewart W J 1999 Magnetism from conductors and enhanced nonlinear phenomena *IEEE Trans. Microw. Theory Tech.* **47** 2075–84

[2] Shelby R A, Smith D R and Schultz S 2001 Experimental verification of a negative index of refraction *Science* **292** 77–9

[3] Linden S, Enkrich C, Wegener M, Zhou J, Koschny Th and Soukoulis C M 2004 Magnetic response of metamaterials at 100 terahertz *Science* **306** 1351–3

[4] Katsarakis N *et al* 2005 Magnetic response of split-ring resonators in the far-infrared frequency regime *Opt. Lett.* **30** 1348–50

[5] Zhang S, Fan W, Minhas B K, Frauenglass A, Malloy K J and Brueck S R J 2005 Midinfrared resonant magnetic nanostructures exhibiting a negative permeability *Phys. Rev. Lett.* **94** 037402

[6] Dolling G, Enkrich C, Wegener M, Soukoulis C M and Linden S 2006 Simultaneous negative phase and group velocity of light in a metamaterial *Science* **312** 892–4

[7] Merlin R 2009 Metamaterials and the Landau–Lifshitz permeability argument: large permittivity begets high-frequency magnetism *Proc. Natl Acad. Sci.* **106** 1693–8

[8] Nils F, Manuel D, Gunnar D, Matthias K W, Stefan L and Wegener M 2007 Photonic metamaterials: new opportunities for nanoimprint *Digest of the 2007 IEEE/LEOS Summer Topical Mtgs* pp 76–7

[9] Zhang S, Fan W, Panoiu N C, Malloy K J, Osgood R M and Brueck S R 2006 Optical negative-index bulk metamaterials consisting of 2D perforated metal–dielectric stacks *Opt. Express* **14** 6778–87

[10] Zhou J, Zhang L, Tuttle G, Koschny T and Soukoulis C M 2006 Negative index materials using simple short wire pairs *Phys. Rev.* B **73** 041101(R)

[11] Alù A, Salandrino A and Engheta N 2006 Negative effective permeability and left-handed materials at optical frequencies *Opt. Express* **14** 1557–67

[12] Menga X, Baia B, Karvinena P, Konishic K, Turunena J, Svirkoa Y and Kuwata-Gonokami M 2008 Experimental realization of all-dielectric planar chiral metamaterials with large optical activity in direct transmission *Thin Solid Films* **516** 8745–8

[13] Hu X, Chan C T, Zi J, Ming Li and Ho K-M 2006 Diamagnetic response of metallic photonic crystals at infrared visible frequencies *Phys. Rev. Lett.* **96** 223901

[14] Economou E N, Koschny T and Soukoulis C M 2008 Strong diamagnetic response in split-ring-resonator metamaterials: numerical study and two-loop model *Phys. Rev.* B **77** 092401

[15] Yao J, Liu Z, Liu Y, Wang Y, Sun C, Bartal G, Stacy A and Zhang X 2008 Optical negative refraction in bulk metamaterials *Science* **321** 930

[16] Jen Y-J, Lakhtakia A, Yu C-W and Lin C-T 2009 Vapor-deposited thin films with negative refractive index in the visible regime arXiv:0903.1177

[17] Podolskiy V A 2003 Plasmon modes and negative refraction in metal nanowire composites *Opt. Express* **11** 735–45

[18] Barnes W L 2006 Surface plasmon-polariton length scales: a route to sub-wavelength optics *J. Opt. A: Pure Appl. Opt.* **8** S87–93

[19] Ghaemi H F, Thio T and Grupp D E 1998 Surface plasmons enhance optical transmission through subwavelength holes *Phys. Rev.* B **58** 6779

[20] Pomplun J, Burger S, Zschiedrich L and Schmidt F 2007 Adaptive finite element method for simulation of optical nano structures arXiv:0711.2149v1
[21] Silveirinha M G, Belov P A and Simovski C R 2007 Subwavelength imaging at infrared frequencies using an array of metallic nanorods *Phys. Rev.* B **75** 035108
[22] Johnson P B and Christy R W 1972 Optical constants of the noble metals *Phys. Rev.* B **6** 43704379
[23] Smith D R and Schultz S 2002 Determination of effective permittivity and permeability of metamaterials from reflection and transmission coefficients *Phys. Rev.* B **65** 195104
[24] Chettiar U K, Kildishev A V, Klar T A and Shalaev V M 2006 Negative index metamaterial combining magnetic resonators with metal films *Opt. Express* **14** 7872–7
[25] Anderson P W 1958 Absence of diffusion in certain random lattices *Phys. Rev.* **109** 1492–505
[26] Wiersma D S, Bartolini P, Lagendijk A and Righini R 1997 Localization of light in a disordered medium *Nature* **390** 671–3
[27] O'Faolain L, White T P, O'Brien D, Yuan X, Settle M D and Krauss T F 2007 Dependence of extrinsic loss on group velocity in photonic crystal waveguides *Opt. Express* **15** 13129–38
[28] Spaldin N 2003 *Magnetic Materials* (Cambridge: Cambridge University Press)
[29] Ying X, Ziyang L, Tao L, Xuxia L, Jieli Z, Jin-Wang H and Liang-Nian J 1999 Magnetic-field-induced Freedericksz transition of a homeotropical alignment liquid crystal doped with double-azo *Japan. J. Appl. Phys.* **38** 6017–8